Additively manufactured negative stiffness structures for shock absorber applications

Additively manufactured Negative Stiffness Structures for shock absorber applications

M. Corsi[1], S. Bagassi[1], M. C. Moruzzi[1], F. Weigand[2]

(1) Department of Industrial Engineering, Università di Bologna, Italy
(2) Arbeitsgruppe Bionic Function and Design, Fraunhofer IAPT, Hamburg, Germany

Keywords:
Negative Stiffness, Additive Manufacturing, Shock Absorber,
Snap-through behaviour, Design of Experiment.

Abstract

Negative stiffness structures (NSS), as a branch of multi-stable mechanical metamaterials, exhibit multiple stable configurations. Their characteristics, such as bi-stability, snap-through and negative stiffness, make them particularly suitable for shock absorber applications. The majority of NSS is designed in a cuboidal shape and only recently few studies focused on cylindrical negative stiffness structures. During this study, three types of special-shaped NSS were designed, produced and tested. To determine the influence of dimensional parameters and materials on the functionality of these flexible structures, for each one of three concepts, five different versions in two different materials and techniques were realized. The specimens were fabricated in PEBA (PolyEther Block Amide) and TPU (Thermoplastic PolyUrethane) using, respectively, Selective Laser Sintering (SLS) and MultiJet Printing (MJP) technologies; the design freedom of Additive Manufacturing (AM), allows the production of complex structures and the possibility of functional integration, such as shock absorber functionality. To investigate the mechanical and NS properties of these structures and their deformation mechanisms, quasi-static compression tests were performed according to ASTM D695 – 15 regulation. The results, analyzed through force-displacement curves, highlighted the energy recovery of the specimens during deformation and the influence of dimensional parameters on the response to the applied loads. During the tests, it was also evident how the usage of different dimensions and materials can lead, for the same structure, to a symmetric or asymmetric buckling mode in the collapse of the layers and to prevent the structure from returning to its original shape once the load has been removed.

1 Introduction

This work is part of a joint project of Fraunhofer IAPT and AKON Robotics, the InspectionCopter. The aim of the project is to design and build a prototype of a copter for inspecting the rotor blades of wind turbines. The InspectionCopter should be equipped with an optical sensor for the resistance measurement of the lightning protection device. To establish a direct contact between the sensor and the rotor blade, the InpectionCopter is equipped with a docking device; a system of vacuum gripper was studied to keep the sensor in position once the Copter is hovering in front of the rotor blades. The docking device avails of a flexible system of pressure springs for shock absorption, as shown in Fig. 1.

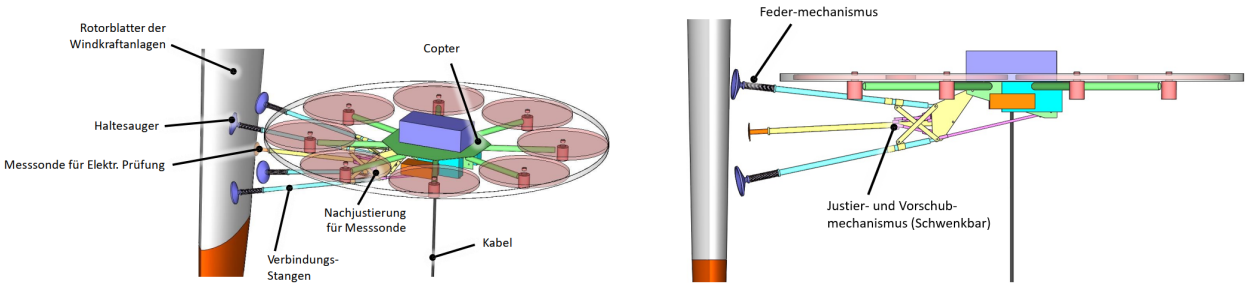

Figure 1: Inspectioncopter preliminary design.

The study performed during the work presented, is intended to explore different types of structures for shock absorption applications that might replace conventional springs. One of the requirements that these structures must satisfy, together with the light weight, is the ability to recover their original shape after the removal of an applied load; to these aims, the best candidates are Negative Stiffness structures produced in polymeric materials through Additive Manufacturing techniques. To find the optimal solution, three types of special-shaped Negative Stiffness Structures were designed, produced and tested.

It was important to characterize the structures by understanding which elements can influence their mechanical performance; to determine the influence of dimensional parameters and materials on the functionality of these flexible structures, for each one of three concepts, five different versions in two different materials and techniques were realized and tested.

In order to reach the goal, the work was divided into different steps. The first step of the work was the design phase; multiple challenges were faced during the realization of the concepts, related both to the functionality and to the subsequent production of the structures. The Design of Experiment (DOE) method, a branch of applied statistics that deals with planning, conducting, analyzing, and interpreting controlled tests to evaluate the factors that control the value of a parameter or group of parameters [1], was the most important tool used during the design phase of the different concepts. The DOE is particularly useful during the design phase of a product when it is necessary to find the optimal value of the variables that influence the behaviour of the system, these variables are called control parameters. The usage of this method allows to identify which control parameters, *factors*, and which combination of factors optimize the results of the process in terms of index of quality. The Design of Experiment aims at the characterization of the system and at the understanding of the cause-effect relation between input and output (*response*) variables to obtain a robust system even in the presence of unpredictable and uncontrollable factors.

The procedure to follow when dealing with the design of parameters can be summarized in two steps:

- Identification of the response of the system, representing the index of quality, and of the influencing input factors.
- Planning of a sufficient amount of tests defining the number of *levels* of the factors at which the response has to be determined.

DoE methodology allows the manipulation of multiple input factors and their levels at the same time, identifying important interactions that might be missed experimenting with *one factor at a time* approach in which certain factors are kept constant and the levels of another variable are alterated. However, it is evident how investigating all the possible combinations, *full factorial*, when the number of factors or levels is relevant, leads to a high amount of tests to perform resulting in significant costs and time. In those cases, it is possible to investigate only a part of the different combinations; this approach is called *fractional factorial*. When this last approach is exploited, the interpolation of the response with mathematical methods allows to find the response even in correspndence of untried combinations ensuring the same result that would have been obtained investigating all the possible combinations.

Once the samples had been produced in PEBA and TPU using, respectively, Selective Laser Sintering and MultiJet Printing technologies all the parts were tested through a quasi-static compression test to verify the conjectures on the influencing factors that were made during the design phase and to investigate how they modify their behaviour in relation to dimensional parameters and materials. Tests and results are reported, respectively, in section 3 and 4. The conclusions and the future developments are illustrated in the final section.

1.1 Negative Stiffness Structures

Materials with effective properties related to the underlying architecture, rather than bulk behaviour of their constituents, are mechanical metamaterials [2]. Elastic instabilities that can cause configurational changes in the microarchitecture of metamaterials were exploited in recent studies [3] to develop tunable metamaterials whose functionality is enhanced with respect to metamaterials with properties that cannot

be tuned. When snap-through instability, a particular kind of elastic instability, is present, a structure switches instantaneously from one stable state to another when an applied stimulus reaches a critical level [4]. This kind of instability is one of the characteristics of Negative Stiffness Structures (NSS), a branch of multi-stable mechanical metamaterials. NSS are mechanical systems that require a decrease in the applied force to generate an increase in displacement [5] (see Fig. 2).

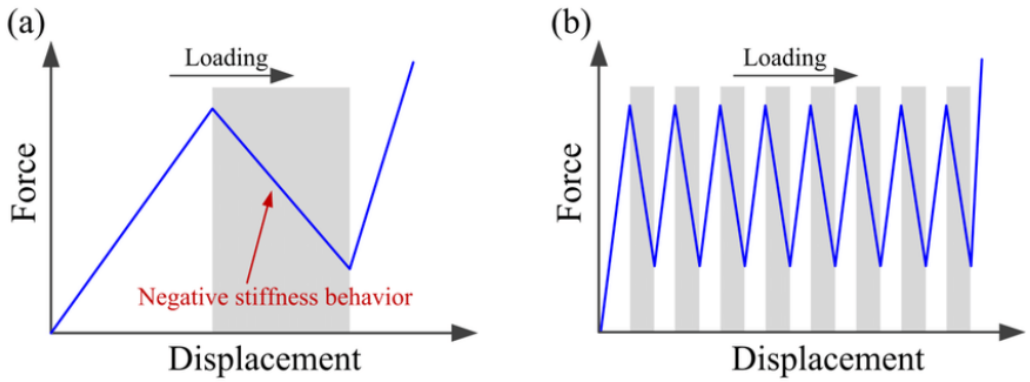

Figure 2: (a) Force-displacement curve of NS element;
(b) force-displacement curve of NS structure.

Their characteristics, such as bi-stability, snap-through and negative stiffness, make them particularly suitable for shock absorber applications; Negative Stiffness elements tend to assist deformation as a result of internally stored energy and so they enhance the damping behaviour. The majority of NSS is designed in a cuboidal shape exploiting the elastic snap-through of a high number of unit cells including pre-shaped curved beams [6, 7, 8, 9] as the one shown in Fig. 3, and only recently few studies focused on cylindrical negative stiffness structures [10].

These curved beams allow for energy recovery as they deform from a buckled shape to another when external load reaches a predetermined threshold (see Fig. 4); this release of energy is revealed in the negative slope of the force - displacement curve.

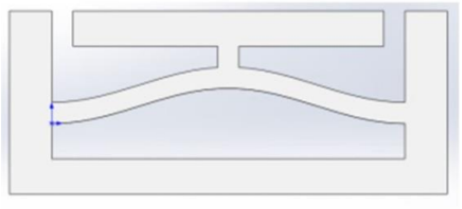

Figure 3: Pre-shaped curved beam.

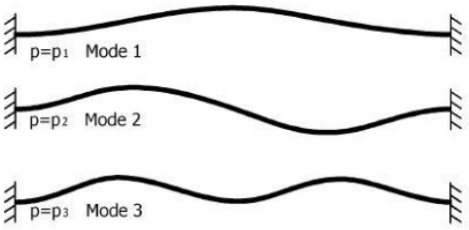

Figure 4: Buckling modes of a curved beam.

2 Apparatus design

The design phase of the structures was the first step of the experimental plan followed by the production and the testing phases. During this study, three types of special-shaped NSS were designed; to determine the influence of dimensional parameters on the functionality of these flexible structures, for each one of three concepts, five different versions were realized.

During the design phase, all the requirements provided by the Fraunhofer IAPT for the realization of desired damping structures were taken into account and respected; additional constraints due to the chosen production technologies were also considered.

The commissioned structures, to be suitable for shock absorber applications, were three, to explore in five different versions and with cylindrical shapes to be fabricated in polymeric materials through AM techniques, specifically, Selective Laser Sintering and Multi Jet Fusion. Albeit in different ways, pre-shaped curved beams are present in all the three structures unit cells to ensure snap-through and bi-stable mechanisms and are expected to exhibit exceptional energy dissipation properties.

Structure A

The first structure (structure A), based on the results presented by Wang et al. [11] was designed through a circular repetition of curved unit cells. Within the cell, the dimensional parameters which were believed to be responsible for the mechanical behaviour of the parts are the apex height of the tilted beams, h, and the wall thickness, t (see Fig. 5); another important factor could have been the number of cells per layer, n. In order to verify these hypotheses, different dimensional combinations were arranged to produce, as requested, five different samples.

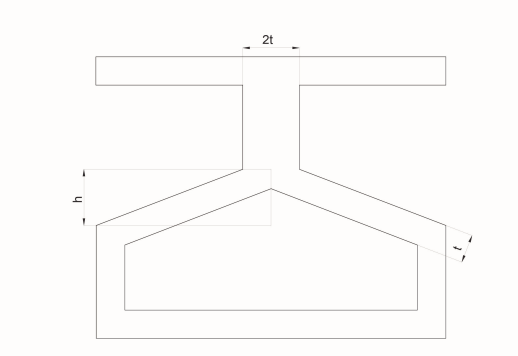

Figure 5: Relevant dimensional parameters of Structure A.

Exploiting a DOE approach, the number of possible combinations was significantly reduced without affecting the conclusion that could have been reached regarding the influence of the dimensional parameters on the mechanical behaviour of the parts.

For structure A, the number of factors is three, namely h, t and n; h and n presents three levels instead of t which has only two levels ($h_1 = 3.00$ mm, $h_2 = 4.00$ mm, $h_3 = 4.50$ mm; $n_1 = 9$, $n_2 = 10$, $n_3 = 12$; $t_1 = 1.00$ mm, $t_2 = 1.50$ mm).

The first concept, realized through the circular repetition of curved unit cells is the only one with the same global dimensions in all of the five samples. In fact, all the different verisons of Structure A, reported in Tab. 1, present an outer radius, R_e, of 30 mm and an inner radius, R_i, of 25 mm and, since

the height of the unit cell is also the same, 15 mm, and the number of layers was set at four, all the A samples share the same nominal height.

Table 1: Parameters Structures A.

Sample	n	t [mm]	h [mm]
A1	10	1.50	3.00
A2	9	1.50	3.00
A3	10	1.00	4.00
A4	9	1.50	4.50
A5	12	1.00	3.00

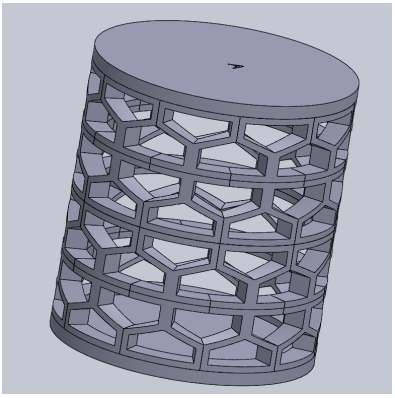

Figure 6: Structure A.

Structure B

The second structure (Structure B) exploits the results obtained by Correra et al. [6] [5], but designing in a brand new way a negative stiffness honeycomb structure. The unit cells were revolved about a vertical axis to obtain a cylindrical part. In this case, the dimensional parameters under investigation are the apex height, h, and the wall thickness and the length of the curved lamella, t and l as it can be seen in Fig. 7.

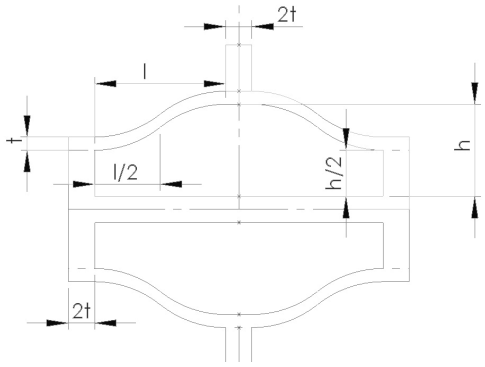

Figure 7: Relevant dimensional parameters of Structure B.

During the design, the three aforementioned factors were varied on different levels ($h_1 = 7.00$ mm, $h_2 = 7.50$ mm, $h_3 = 8.00$ mm, $h_4 = 8.50$ mm; $t_1 = 1.00$ mm, $t_2 = 1.50$ mm, $t_3 = 2.00$ mm; $l_1 = 10.00$ mm, $l_2 = 11.00$ mm, $l_3 = 12.00$ mm); the possible combinations were thirty-six, but the DOE approach was exploited to reduce the number of samples to five.

In the second concept, the desired cylindrical structure was obtained rotating a well-known NS honeycomb structure [5]. The major design challenge for this structure was to overcome the manufacturing constraints. In order to face this challenge, discontinuities in both the internal and external shape were included to allow residual powder removal in the post-processing production phase. The external shape presents two holes per layer, the minimum allowable diameter of these holes represented a limitation for the minimum reachable dimensions of the apex height, h. To avoid stress concentrations along the same axis, the holes were placed in different positions on different layers. For the same purpose, the unit cells were put in communication providing the common bases with some cuts as shown in Fig. 8.

Figure 8: Residual powder removal points.

The different samples of Structure B are listed in the table below (Tab.2)

Table 2: Parameters Structures B.

Sample	l [mm]	h [mm]	t [mm]
B1	10.00	7.00	1.00
B2	11.00	7.00	1.50
B3	12.00	8.50	2.00
B4	11.00	7.50	1.00
B5	12.00	8.00	1.50

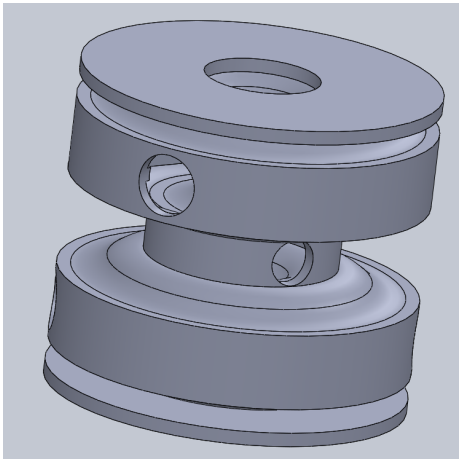

Figure 9: Structure B.

Structure C

The third structure, Structure C, was been designed through a circular repetition of unit cells of elliptic shape. Unlike structures A and B, this concept is not based on previous studies and so the number of factors that were investigated is higher. It was acted on the following dimensional parameters of the cell: the wall thickness, t, the depth, d, and the semimajor axis and the distance between the foci, respectively a and c (see Fig. 10).

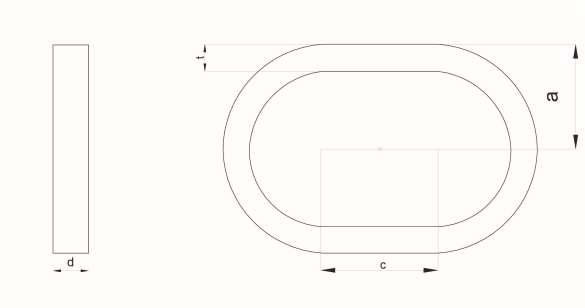

Figure 10: Relevant dimensional parameters of Structure C.

In this last case, the usage of the DOE brought the greatest benefits. Considering all the levels for each factor ($t_1 = 1.50$ mm, $t_2 = 2.00$ mm; $d_1 = 1.50$ mm, $d_2 = 2.00$ mm, $d_3 = 3.00$ mm; $a_1 = 5.00$ mm, $a_2 = 6.00$ mm, $a_3 = 6.50$ mm, $a_4 = 7.00$ mm; $c_1 = 3.00$ mm, $c_2 = 5.00$ mm, $c_3 = 6.00$ mm), it can be seen how the number of possible samples has been reduced from seventy-two to five.

The last concept, as stated before, was realized through a circular repetition of elliptical unit cells; the number of cells for each one of the two layers was set to six and alternated with an angle of 60° from one layer to the other, keeping a constant outer radius of 20 mm. All the designed concepts are listed in the table below Tab. 3.

Table 3: Parameters Structures C.

Sample	c [mm]	a [mm]	d [mm]	t [mm]
C1	5.00	6.50	2.00	2.00
C2	6.00	7.00	1.50	2.00
C3	5.00	6.50	3.00	1.50
C4	6.00	6.00	2.00	1.50
C5	3.00	5.00	2.00	1.50

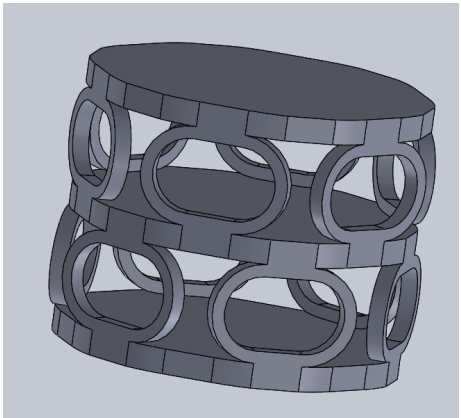

Figure 11: Structure C.

2.1 Production

All samples were produced through AM techniques, namely SLS and MJP using respectively, PrimePart® ST (PEBA 2301) and Ultrasint® TPU01 materials. AM offers design freedom and the possibility of functional integration so it perfectly fits the goal of integrating shock absorber functionality in the implementation of these new, complex damping structures. Parts produced with PEBA material, possess excellent material properties, such as high elasticity and strength and excellent long term stability; these features together with its rubber-like fatigue behaviour make PEBA a great material for fully functional applications, flexible plastic parts of high quality for long term use [12]. Parts created from TPU material possess great accuracy, high flexibility and shock absorption. TPU is particularly suitable for producing lattice structures and functional and design prototypes [13]. The choice to produce the structures in two different materials was taken to investigate how the material affects their mechanical behaviour.

The samples in PEBA material (Fig. 12, 14, 16), were printed through the SLS technique.

The samples in TPU material (Fig. 17, 15, 16), were printed through the MJP technique.

Figure 12: Structures A in PEBA.

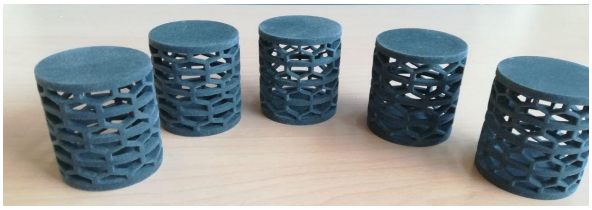

Figure 13: Structures A in TPU.

Figure 14: Structures B in PEBA.

Figure 15: Structures B in TPU.

Figure 16: Structures C in PEBA.

Figure 17: Structures C in TPU.

Table 4 sets out the height (nominal and real) and the mass of each part.

Table 4: Height and mass of the structures.

Sample	Nom. height [mm]	Real height [mm]		Mass [g]	
		PEBA	TPU	PEBA	TPU
A1	66.00	64.21	64.31	34.80	42.50
A2	66.00	65.10	64.00	36.40	42.50
A3	66.00	65.47	64.13	32.70	39.50
A4	66.00	65.80	64.61	36.30	41.90
A5	66.00	65.30	64.15	35.40	39.20
B1	47.00	47.10	46.07	25.60	33.10
B2	51.00	50.53	51.55	49.00	65.40
B3	62.50	62.70	61.58	83.20	108.60
B4	49.50	49.50	48.46	29.80	38.30
B5	55.00	54.50	54.50	54.60	76.30
C1	38.00	37.21	37.85	18.40	21.50
C2	40.00	39.97	39.44	17.90	21.70
C3	35.00	33.84	33.69	14.90	17.20
C4	33.00	32.46	32.62	14.20	16.50
C5	29.00	28.90	28.03	13.40	15.10

3 Methods

3.1 Quasi-static compression test

Quasi-static compression tests were performed, using a universal testing machine, on the 30 samples, according to ASTM 695-15 regulation, to investigate both the mechanical properties of the structures and the influence of the different dimensional parameters and materials. Each sample was tested just once since, as a first approach, it was important to understand the trend of the response and not to characterize the structures. The data was acquired with the same parameters for all the different structures:

- *Load Cell* : 10 kN
- *Crosshead Speed* : 0,0176 mm/s
- *Sample Rate*: 1000 Hz
- *Scan Rate*: 500 Hz
- *Sample to Read*: 2

The outcome of the test was a Force-Displacement curve, the acquisition phase was stopped once the curve presented a constant slope or, as in the case of some of the Structure C, when the unit cells failed. The test execution was divided in two batches according to the material; the first one for the PEBA and the second one for the TPU. First conclusions on the behaviour of the structures were reached looking at the deformation mode, both local of the pre-shaped beams and global of the entire part, they achieved under uniaxial compression.

To better explain how the different layers collapse during the tests, the name of the layers of each structure is set out in Figures 18, 19 and 20.

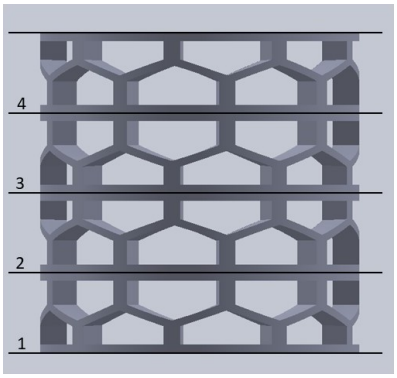

Figure 18: Nomenclature of layers in structure A.

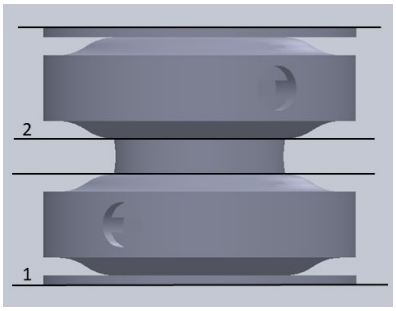

Figure 19: Nomenclature of layers in structure B.

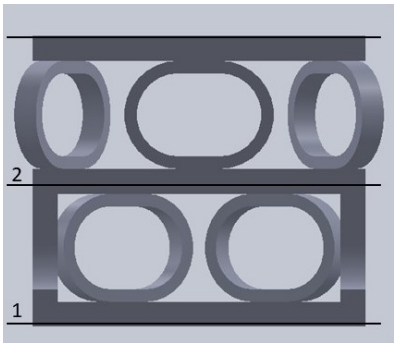

Figure 20: Nomenclature of layers in structure C.

Structure A

The tests performed on the ten samples of structure A present a sequence of collapse of the layers that was unpredictable; it depends on the printing quality. Each layer of the structure has a different strength so the collapse of the layers procedes from the weakest to the strongest. During the compacting phase, the structure can exhibit two different deformation modes, local and global. The local mode is related to the buckling of the curved beams that can be symmetric or asymmetric and is due to the twist of the central support bar. The global one, instead, is referred to the out-of-plane deformation of the whole structure and is a consequence of the span of the curved beam that increases along the radial direction and causes an uneven distribution of stresses between the interior and the exterior part of the cells.

Two of the samples, namely A3 and A5 in PEBA material, showed a bistable configuration; once the acquisition was stopped, the structures did not recovered to their initial shape, but displayed a bistable behaviour remaining in a new stable position.

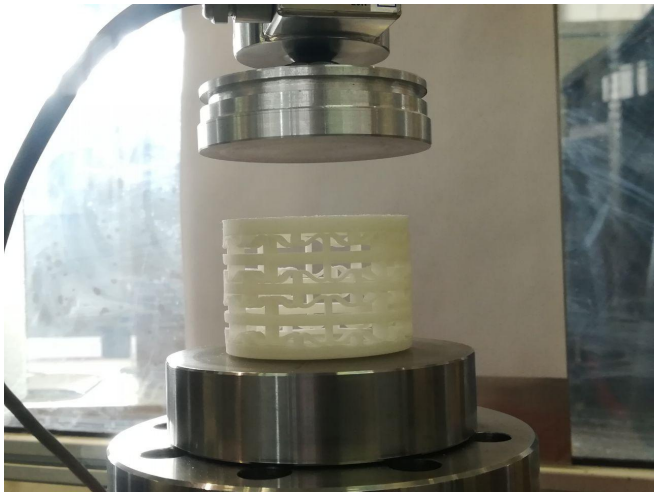

Figure 21: New stable position of Sample A3 in PEBA.

Structure B

All the five samples of Structure B in either PEBA and TPU exhibited the same sequence in the collapse of the layers; at first, the upper part of layer 1 collapsed, followed by the bottom part of layer 2. None of the structures presented out-of-plane deformation.

Structure C

During the tests, all the structures C in PEBA material failed along the lobes of the unit cells and so the acquisitions were stopped before reaching the maximum allowable displacement.

Structures C in TPU material, in contrast to the ones in PEBA material, did not fail under compression, making it possible to compact them till the point of maximum allowable displacement. Compared to all the other types of structures, some of these parts, namely Samples C1, C2 and C4, showed an important out-of-plane deformation that can be seen in Fig. 22.

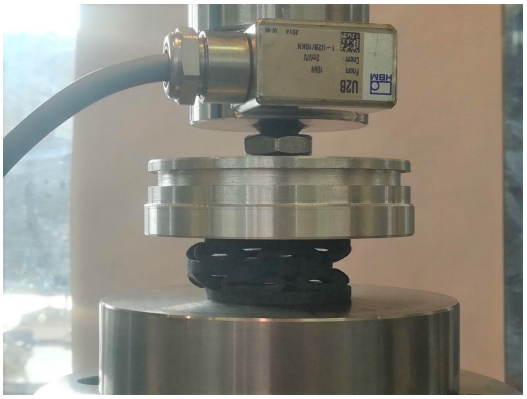

Figure 22: Deformation of Sample C5 in TPU.

4 Results and discussion

This section presents the results related to the displacement and the load of the structures. Through the comparison of the test performed on the five different samples for each structure type it was possible to determine the dimensional parameters that most affect their behaviour, and comparing the load-displacement curves of the same samples in PEBA and TPU, conclusions were reached regarding the effect of the material. Moreover, looking at Table 5, it can be notced how the height of the samples has slightly decreased after the test. Ultimately, it was decided to define a relative strength, normalizing the load applied to the structures at 50% of the displacement with respect to the weight force, as merit index.

Table 5: Final height, load at 50% of displacement, weight, merit index.

Sample	Final height [mm]		Load at 50% of disp. [N]		Weight [N]		Merit index	
	PEBA	TPU	PEBA	TPU	PEBA	TPU	PEBA	TPU
A1	64.12	64.22	$3.00\text{x}10^{1}$	$6.20\text{x}10^{1}$	$34.13\text{x}10^{-2}$	$41.69\text{x}10^{-2}$	$8.79\text{x}10^{1}$	$1.49\text{x}10^{2}$
A2	64.00	62.64	$2.39\text{x}10^{1}$	$5.08\text{x}10^{1}$	$35.70\text{x}10^{-2}$	$41.69\text{x}10^{-2}$	$6.69\text{x}10^{1}$	1.2210^{2}
A3	65.07	63.55	$1.10\text{x}10^{1}$	$1.95\text{x}10^{1}$	$32.07\text{x}10^{-2}$	$38.74\text{x}10^{-2}$	$3.43\text{x}10^{1}$	5.0310^{1}
A4	65.70	63.34	$2.28\text{x}10^{1}$	$5.36\text{x}10^{1}$	$35.61\text{x}10^{-2}$	$41.10\text{x}10^{-2}$	$6.40\text{x}10^{1}$	$1.30\text{x}10^{2}$
A5	65.11	63.65	$2.50\text{x}10^{1}$	$5.58\text{x}10^{1}$	$34.72\text{x}10^{-2}$	$38.45\text{x}10^{-2}$	$7.20\text{x}10^{1}$	$1.45\text{x}10^{2}$
B1	46.27	45.30	$2.94\text{x}10^{1}$	$4.33\text{x}10^{1}$	$25.11\text{x}10^{-2}$	$32.47\text{x}10^{-2}$	$1.17\text{x}10^{2}$	$1.33\text{x}10^{2}$
B2	50.00	49.90	$6.01\text{x}10^{1}$	$14.06\text{x}10^{1}$	$48.06\text{x}10^{-2}$	$64.15\text{x}10^{-2}$	$1.25\text{x}10^{2}$	$2.19\text{x}10^{2}$
B3	60.55	61.00	$12.18\text{x}10^{1}$	$21.91\text{x}10^{1}$	$81.61\text{x}10^{-2}$	$106.53\text{x}10^{-2}$	$1.49\text{x}10^{2}$	$2.05\text{x}10^{2}$
B4	48.57	47.10	$2.10\text{x}10^{1}$	$3.52\text{x}10^{1}$	$29.23\text{x}10^{-2}$	$37.57\text{x}10^{-2}$	$7.18\text{x}10^{1}$	$9.37\text{x}10^{1}$
B5	53.46	53.80	$4.97\text{x}10^{1}$	$7.97\text{x}10^{1}$	$53.56\text{x}10^{-2}$	$74.80\text{x}10^{-2}$	$9.28\text{x}10^{1}$	$1.06\text{x}10^{1}$
C1	36.47	36.86	$3.40\text{x}10^{1}$	$8.36\text{x}10^{1}$	$18.05\text{x}10^{-2}$	$21.09\text{x}10^{-2}$	$1.88\text{x}10^{2}$	$3.96\text{x}10^{2}$
C2	38.56	38.78	$3.36\text{x}10^{1}$	$5.55\text{x}10^{1}$	$17.55\text{x}10^{-2}$	$21.28\text{x}10^{-2}$	$1.90\text{x}10^{2}$	$2.51\text{x}10^{2}$
C3	32.61	32.90	$4.68\text{x}10^{1}$	$8.56\text{x}10^{1}$	$14.61\text{x}10^{-2}$	$16.87\text{x}10^{-2}$	$3.20\text{x}10^{2}$	$5.07\text{x}10^{2}$
C4	31.51	31.41	$2.74\text{x}10^{1}$	$5.20\text{x}10^{1}$	$13.93\text{x}10^{-2}$	$16.18\text{x}10^{-2}$	$1.96\text{x}10^{2}$	$3.21\text{x}10^{2}$
C5	27.80	27.25	$3.42\text{x}10^{1}$	$5.55\text{x}10^{1}$	$13.14\text{x}10^{-2}$	$14.81\text{x}10^{-2}$	$2.60\text{x}10^{2}$	$3.75\text{x}10^{2}$

4.1 Effect of dimensional parameters

Structure A

All the samples of Structure A exhibit a negative stiffnes behaviour. All the curves present the typical shape of NSS Load - Displacement curve; an initial deformation phase is followed by the elastic instability phase where the curved beams of the cells snap-through. These two phases are repeated for each layer and each peak corresponds to the collapse of one layer; the different height of the peaks is due to the different strength of each layer own to the printing process. The last phase is the compacting one which shows a positive slope of the curve. Looking at the trend of the different curves, Fig. 23, it is easy to see how the dimensional parameter that seems to have a greater impact on the mechanical behaviour of this type of structure is the apex height. Samples A1 and A2 differ only for the number of unit cells and present almost the same shape at the same load values. Samples A2 and A4 that have the same number of cells and the same wall thickness, instead, present an important difference in terms of load; increasing the value of h, apex height, the negative stiffness properties are enhanced. Sample A5 has a trend which is quite different from the other four parts and it is the one with the lowest number of cells. It is interesting to notice how the two samples with the same wall thickness A3 and A5 are the ones that did not recover their original shape at the end of the tests.

Considering the Force - Displacement curves of structures A in TPU material, a more severe NS behaviour was noticed in those samples with a higher ratio between the apex height, h, and the wall thickness, t. In structures with a low value of this ratio, the number of cells becomes more important leading to a weak Negative Stiffness behaviour.

Structure B

All the parts of Structure B in PEBA material exhibit the same trend of the curves, Fig. 24. The analysis of the results seems to confirm the conclusions of Correra et al. [5] that states that the Negative Stiffness behaviour is linked to the ratio between the apex height, h, and the wall thickness, t. It is interesting to note that in the case of a circular structure, the wall thickness has a greater influence. Even if the aforementioned ratio is almost the same in Samples B2 and B3, 4.25 and 4.26 respectively, the load reached in this last sample is much higher than the one of Sample B2. This behaviour might depend on the relation between the wall thickess of the curved beam and the one of the outer wall (see Fig. 7); an increase of this last parameter leads to an increase of the load.

Structures B fabricated in TPU material, do not exhibit a NS behaviour, but even in this case, as for the

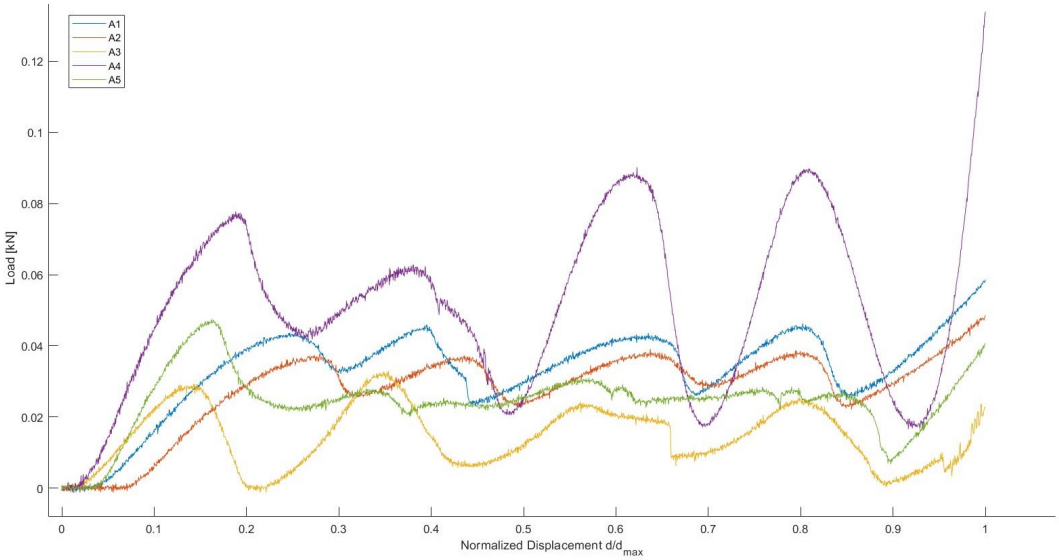

Figure 23: Force - Normalized Displacement curve of Structures A in PEBA.

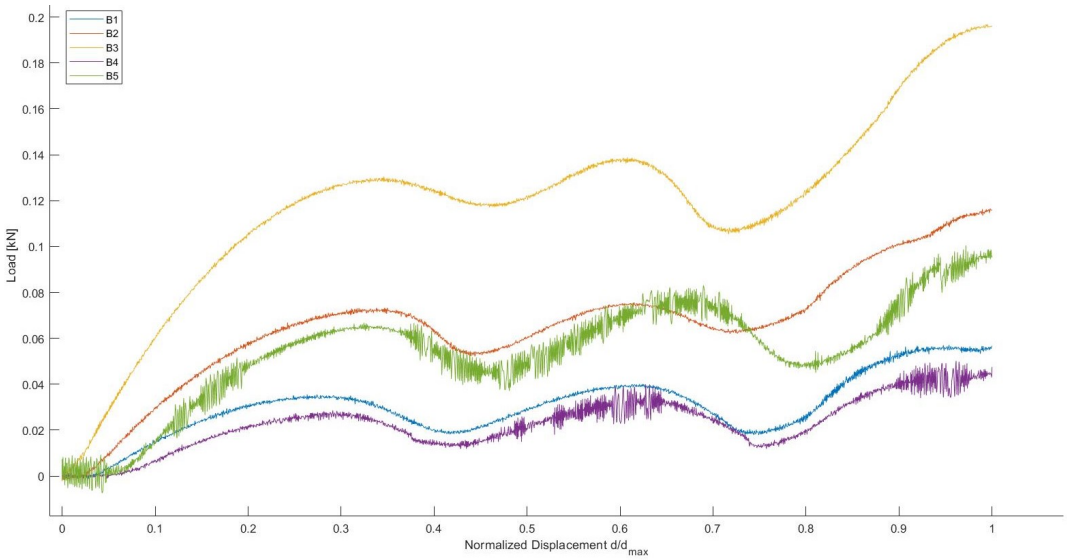

Figure 24: Force - Normalized Displacement curve of Structures B in PEBA.

same samples in PEBA material, the dimensional parameters with a greater influence on the mechanical behaviour seem to be the wall thickness, t, and the ratio between the apex height and t. Samples with almost the same aforementioned ratio show the same trend of the curves and considering samples that share the same value of wall thickness, B1 and B4, the Force - Displacement curves are even almost coincident.

Structure C

Structures C, in either PEBA and TPU, do not exhibit a negative stiffness behaviour, the slope of the curves is almost constant and positive. Looking at the different curves, the dimensional parameter that seems to influence the behaviour of the structure is the depth of the cell, d.

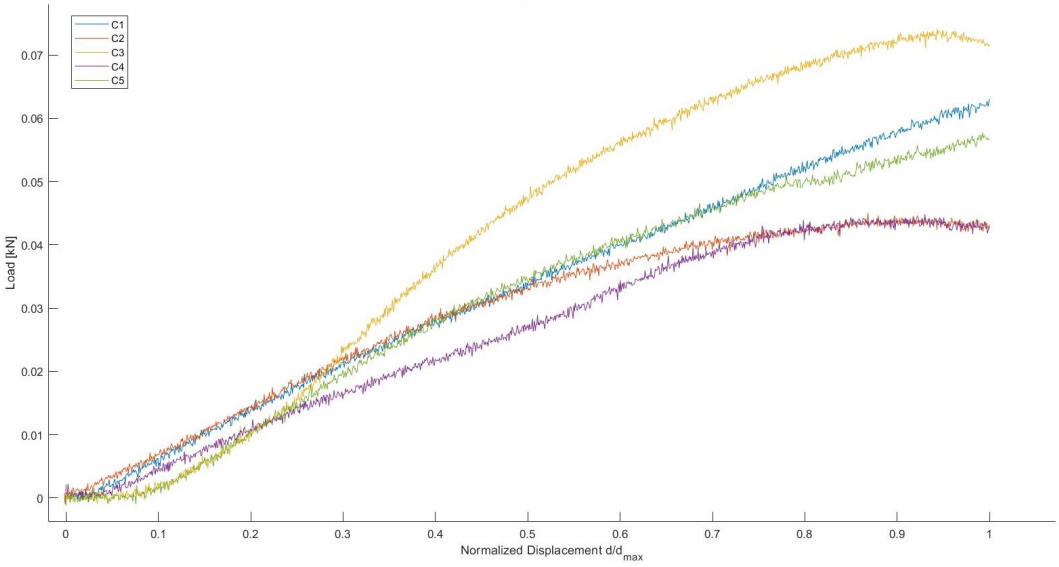

Figure 25: Force - Normalized Displacement curve of Structures C in PEBA.

4.2 Effect of material

Once the influence of dimensional parameters on the mechanical behaviour of the structures has been defined, a comparison between the same parts in the two different materials can also be performed. Looking at the figure below, Fig. 26, it is possible to see how the usage of TPU leads to an increase of load with respect to PEBA for the same displacement value; so, for structures fabricated in PEBA material, high displacement values can be achieved with a low applied load.

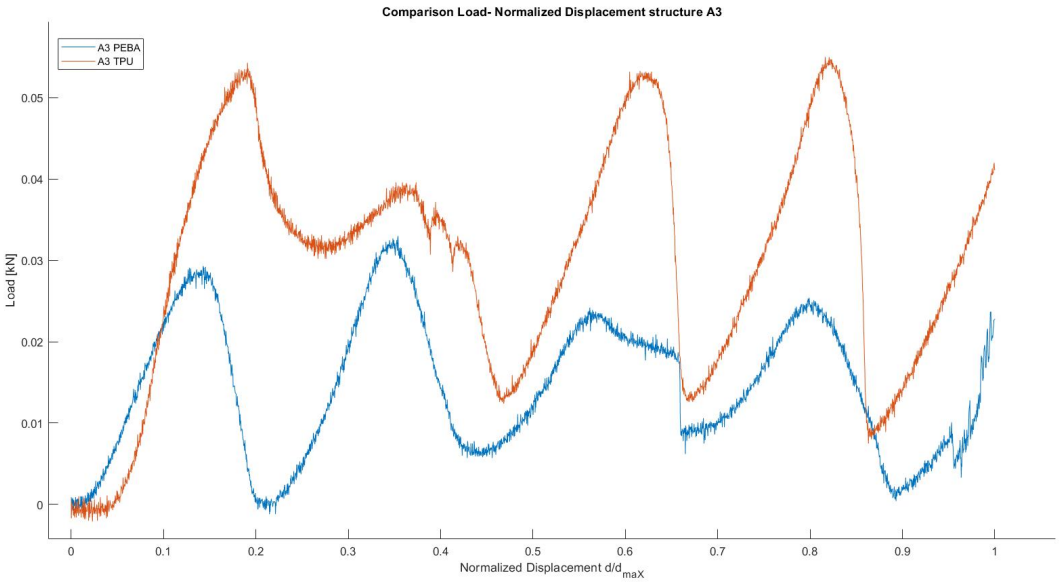

Figure 26: Force-Normalized Displacement curve Comparison of Structure A3 in PEBA and TPU.

4.3 Merit index

Since all the three structures presented in this study exploit innovative shapes, it is not possible to use the conventional indices of merit referred to bulk structures. Finding new ways to describe unconventional structures was one of the challenges faced during this work and, in general, anytime a special-shaped part is involved. With reference to the InspectionCopter project, and aeronautical applications in general, where weight reduction is one of the main objectives for structural optimization, it was decided to define a relative strength normalizing the load applied to the structures at 50% of the displacement with respect to their weight force; in this way the obtained coefficients, listed in Table 5, turn out to be dimensionless.

5 Conclusions

During the study presented in this work, different types of structures intended to replace conventional springs in shock absorption applications were explored. The main goal of the investigation was to understand how the dimensional parameters and materials affect the mechanical behaviour and consequently the functionality of these structures. Since the two main requirements these structure had to satisfy were ability to recover their original shape despite undergoing compression to the point of densification and the light weight, it was decided to design parts with Negative Stiffness behaviour to be produced in polymeric materials through Additive Manufacturing techniques. During the design phase, a Design of Experiment approach was exploited to significantly reduce the number of possible tests, with different combinations of those dimensional parameters of the constituting unit cells that might have been responsible for the mechanical performance. For each one of the three concepts of the special-shaped Negative Stiffness Structures, five different versions in two different materials and AM techniques were realized.

Important conclusions were reached looking at the results of the Quasi-static compression tests performed on the structures according to ASTM 695-15 regulation. In structures A and B, the most influencing parameters seemed to be the apex height, the thickness of the pre-shaped beams and their ratio. In structures A fabricated in TPU, the number of cells per layer gained more relevance when the aforementioned ratio was lower; in those cases, to obtain a NS behaviour, a higher number of cells was necessary. Another important characteristic of some of the samples A was found in those parts with the lowest value of wall thickness; samples A3 and A5 in PEBA material did not recover their initial shape and remained in a new stable configuration after the load removal. For the structures in TPU, this bistable behaviour was not present except in a few instants in the sample A3. In structures B fabricated in PEBA material, NS behaviour was not so prominent and in TPU material it was not present at all. Structures C in either PEBA and TPU did not reveal NS characteristics and in the first case, all the parts failed during the execution of the Quasi-static compression tests.

It is possible to conclude that the structure that better performs and satisfies the NS behaviour requirement is Structure A.

Future works should focus on a deeper investigation of Structure A looking for other parameters that may play a role on its behaviour, such as the dimension of the inner and outer radii R_i and R_e. The depth of the unit cell, in fact, proved to be the influencing parameter in Structures C.

To demonstrate the feasibility of these parts for shock absorbtion applications, additional experiments should be performed, in particular loading-unloading tests to evaluate the energy absorbtion capability, a key factor in damping structures. Fig. 27 shows a possible application of structure A and B, replacing the conventional spring, in the optical sensor of the InspectionCopter.

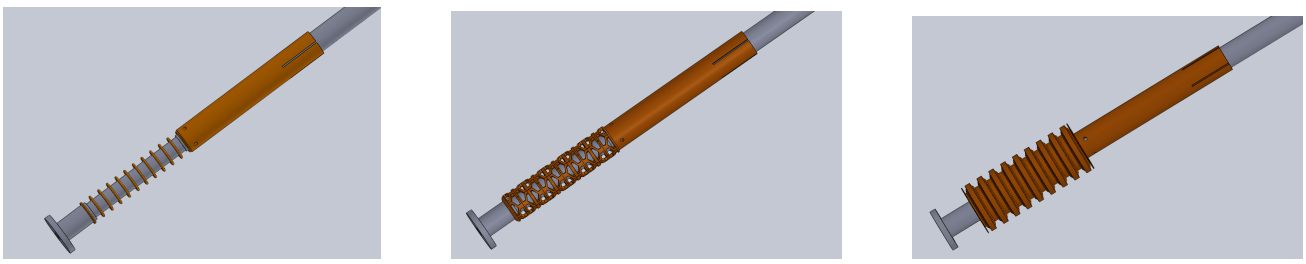

Figure 27: Possible applications of structure A and B in the optical sensor of the InspectionCopter.

References

[1] ASQ. *quality resources, design of experiment.* https://asq.org/quality-resources/design-of-experiments.

[2] Kaikai Che, Chao Yuan, Jiangtao Wu, H Jerry Qi, and Julien Meaud. Three-dimensional-printed multistable mechanical metamaterials with a deterministic deformation sequence. *Journal of Applied Mechanics*, 84(1), 2017.

[3] Nan Hu and Rigoberto Burgueño. Buckling-induced smart applications: recent advances and trends. *Smart Materials and Structures*, 24(6):063001, 2015.

[4] George Simitses and Dewey H Hodges. *Fundamentals of structural stability.* Butterworth-Heinemann, 2006.

[5] Dixon M Correa, Timothy Klatt, Sergio Cortes, Michael Haberman, Desiderio Kovar, and Carolyn Seepersad. Negative stiffness honeycombs for recoverable shock isolation. *Rapid Prototyping Journal*, 2015.

[6] Dixon M Correa, Carolyn Conner Seepersad, and Michael R Haberman. Mechanical design of negative stiffness honeycomb materials. *Integrating Materials and Manufacturing Innovation*, 4(1):10, 2015.

[7] Lia Kashdan, Carolyn Conner Seepersad, Michael Haberman, and Preston S Wilson. Design, fabrication, and evaluation of negative stiffness elements using sls. *Rapid Prototyping Journal*, 2012.

[8] Chenhui Ren, Deqing Yang, and Haoxing Qin. Mechanical performance of multidirectional buckling-based negative stiffness metamaterials: an analytical and numerical study. *Materials*, 11(7):1078, 2018.

[9] Hang Yang and Li Ma. Multi-stable mechanical metamaterials with shape-reconfiguration and zero poisson's ratio. *Materials & Design*, 152:181–190, 2018.

[10] Xiaojun Tan, Bing Wang, Shuai Chen, Shaowei Zhu, and Yuguo Sun. A novel cylindrical negative stiffness structure for shock isolation. *Composite Structures*, 214:397–405, 2019.

[11] Bing Wang, Xiaojun Tan, Shaowei Zhu, Shuai Chen, Kaili Yao, Peifei Xu, Lianchao Wang, Huaping Wu, and Yuguo Sun. Cushion performance of cylindrical negative stiffness structures: Analysis and optimization. *Composite Structures*, 227:111276, 2019.

[12] eos. *PrimePart ST PEBA 2301.* https://www.eos.info/material-p.

[13] Basf. *Ultrasint TPU01.* https://www.basf.com/global/en/who-we-are/organization/locations/europe/german-companies/basf-3d-printing-solutions-gmbh/powders/Ultrasint_TPU01.html.